Available online at www.sciencedirect.com

ScienceDirect

Procedia Manufacturing 35 (2019) 666–673

Procedia MANUFACTURING

www.elsevier.com/locate/procedia

2nd International Conference on Sustainable Materials Processing and Manufacturing

(SMPM 2019)

Effect of atmospheric aerosol on corrosion of metallic surfaces

Emetere M.E.*[a,c], Okoro E.E.[b] , Akinlabi E.T.[c] and Sanni S.E. [d]

[a]*Department of Physics, Covenant University Canaan land, P.M.B 1023, Ota, Nigeria.*
[b]*Department of Petroleum Engineering, Covenant University Canaan land, P.M.B 1023, Ota, Nigeria*
[c]*Department of Mechanical Engineering Science, University of Johannesburg, South Africa.*
[d]*Department of Chemical Engineering, Covenant University Canaan land, P.M.B 1023, Ota, Nigeria*

Abstract

This research investigates the impact of atmospheric aerosols to initiate atmospheric corrosion of metallic surfaces. Fifteen years' primary (aerosol optical depth) dataset was obtained from the Multi-Angle Imaging Spectro-Radiometer (MISR). Aerosol loading were generated from the primary dataset. The component of the atmospheric aerosols was obtained from existing literature. A mathematical projection on the corrosion of metallic surfaces was done using spatial maps and secondary dataset. The yearly corrosion rate has doubled since 2004. Higher accuracy of the modified Faraday model can be achieved using ground dataset.

Peer-review under responsibility of the organizing committee of SMPM 2019.

Keywords: aerosol, aerosol loading, corrosion, atmospheric corrosion

1. Introduction

The behavioral pattern of atmospheric aerosol particle in outdoor environments is largely known due to the knowledge of atmospheric forces that controls its transport and loading [1-3]. Aerosol loading concept describes the pattern which atmospheric aerosols are retained in the atmosphere for as long as their life time [4-5]. The classification of atmospheric aerosols can be via its sizes and composition. Atmospheric aerosols are considered as

*Corresponding Author
Email: emetere@yahoo.com

2351-9789
Peer-review under responsibility of the organizing committee of SMPM 2019.
10.1016/j.promfg.2019.06.008

one of the main factor in atmospheric corrosion. This is because aerosols are composed of chemical compounds (e.g. SO2, CO, NO2, CO2) that initiates the corrosion processes in exposed metals (Figure 1).

Figure 1: Atmospheric corrosion that is initiated by atmospheric particles

There are research works on how meteorological variables and environmental pollutants affect corrosion of metallic surfaces [6-7]. The chemical reaction from pollutants – leading to corrosion is expressed in Figure 2. Most aerosols are deposited near shorelines due to dispersion patterns that is assisted with wind activities [2]. Hence, aside the humidity in shorelines, atmospheric aerosols play vital role in corrosion [8].

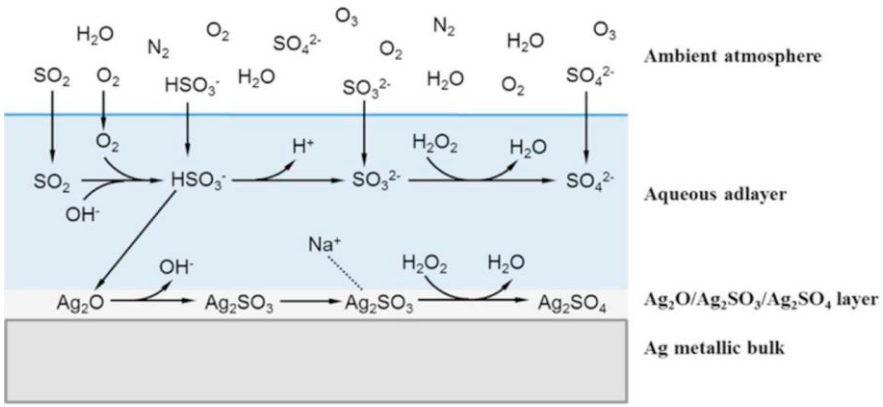

Figure 2: effects of environmental pollutants on corrosion

The primary data was obtained from Multi-angle Imaging Spectro-Radiometer (MISR). The secondary dataset was obtained using the West African regional scale dispersion model (WASDM) from the AOD dataset.

2. Materials and Methods

The research location is Dori in Burkina Faso. Dori is located on latitude 14.03°N and longitude 0.03°W. (Figure 1). The West African regional scale dispersion model (WASDM) was used to estimate the aerosol loading over a region. WASDM for aerosol loading is given as:

$$\psi(\lambda) = a_1{}^2 \cos\left(\frac{n_1 \pi \tau(\lambda)}{2} x\right) \cos\left(\frac{n_1 \pi \tau(\lambda)}{2} y\right) + \cdots \ldots a_n{}^2 \cos\left(\frac{n_n \pi \tau(\lambda)}{2} x\right) \cos\left(\frac{n_n \pi \tau(\lambda)}{2} y\right) \quad (1)$$

a is atmospheric constant gotten from the fifteen years aerosol optical depth (AOD) dataset from MISR, n is the tunning constant, $\tau(\lambda)$ is the AOD of the area and $\psi(\lambda)$ is the aerosol loading.

The digital voltage and Angstrom parameters of the study area can be obtained from equations (2) and (3) respectively.

$$I(555) = \frac{I_0(555)}{R^2} \exp(m * \tau(555)) \quad (2)$$

where I s the solar radiance over the SPM detector at wavelength λ = 555 nm, Io is the is a measure of solar radiation behind the atmosphere, R is the mean Earth-Sun distance in Astronomical Units, τ is the total optical depth (in this case, the average of the each month is referred to as the total AOD, and m is the optical air mass.

$$\alpha = -\frac{d\,In\,(\tau)}{d\,In\,(\lambda)} \quad (3)$$

where α is the Angstrom parameter, τ is the aerosol optical depth, and λ is the wavelength. The radius of the particles for atmospheric aerosol and back-envelope was calculated using proposals by Kokhanovsky et al [9]. The analysis of equations (1) was done using the C++ codes.

The atmospheric corrossion rate of metals over the Dori was calculated using the Faraday equation [10]. It is given as :

$$CR\ \left(\frac{\mu m}{yr}\right) = k \frac{i_{corr}}{d} EW \quad (4)$$

Where k is a conversion factor (3.27 x 10^6 μm·g·A^{-1}·cm^{-1}·yr^{-1}), i_{corr} is the corrosion current density in μA/cm² (calculated from the measurements of Rp), EW is the equivalent weight, and d is the density of Alloy 22 (8.69 g/cm³).

Based on equation (4), the modification in the work is the inclusion of aerosol loading.

$$CR\ \left(\frac{\mu m}{yr}\right) = k \frac{i_{corr}}{d} EW / \exp\left(\frac{EW * \psi(\lambda)}{2.32}\right) \quad (5)$$

In this study, the corrosion current density of iron was considered and it is given as 3.2 x10^{-3} μA/cm². The EW of iron is given as 27.9225.

3. Results and Discussion

The spatial distribution of the aerosol optical depth (AOD) was obtained from Multi-angle Imaging Spectro-Radiometer (MISR) is presented in Figure 3. It shows that the impact of the atmospheric corrosion on metallic surfaces would be at the center of the city. The aerosol loading that was derived from the West African

regional scale dispersion model (WASDM) is presented in Figure 4. It can be shown that the wind activities over the region may shift the impact of atmospheric corrosion towards the north-east of the location. The angstrom exponent which describe the dependency of the AOD on wavelength is presented in Table 1. The radius of particle (back of envelope calculation) is presented in Table 2. Figure 5 presents the radius of particle (atmospheric aerosols). The sizes of aerosols determines the deposition rate of aerosols over an exposed metal surface. It can be inferred from the saptial distribution shown in Figure 5 that the sizes of aerosols follows same pattern as the AOD. The statistics of the AOD data presented in Table 3. The corrosion rate over Dori on iron metallic surfaces is presented in Figure 6.

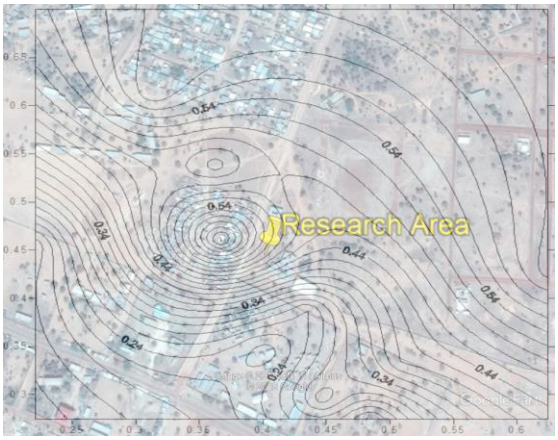

Figure 3: Spatial map of Dori (AOD)

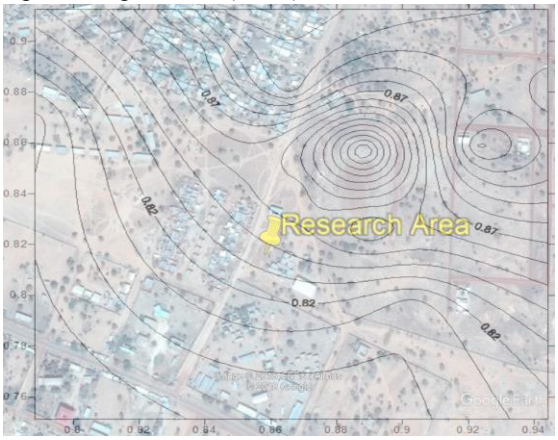

Figure 4: Spatial map of Dori (Aerosol loading)

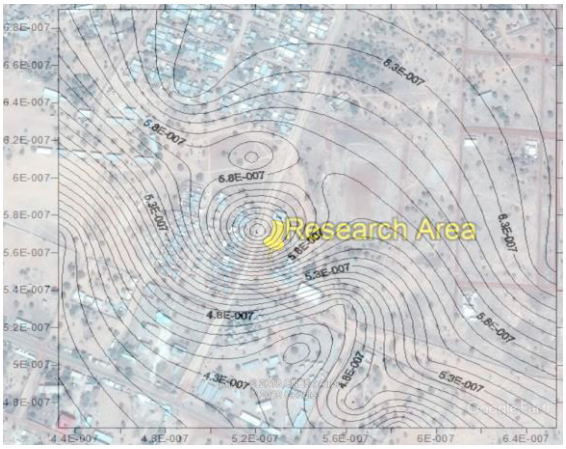

Figure 5: Spatial map of Dori (Aerosol size)

Table 1: Angstrom parameter over Dori

Month	2000	2001	2002	2003	2004	2005	2006	2007	2008	2009	2010	2011	2012	2013
Jan		0.144	0.169	0.250	0.216	0.085	0.181	0.240	0.225	0.232	0.300	0.229	0.244	0.309
Feb		0.128	0.193	0.173	0.113	0.144	0.194	0.204	0.258	0.053	0.251	0.206	0.100	0.316
Mar	0.075	0.135	0.073	0.061	0.024	0.037	0.097	0.089	0.140	0.026	0.066	0.032	0.019	0.149
Apr	0.075	0.057	0.071	0.047	0.025	0.055	0.074	0.023	0.033	0.105	-0.029	0.098	0.040	0.059
May	0.184	0.078	0.082	0.077	0.118	0.073	0.070	0.042	0.144	0.107	0.037	0.067	0.037	0.120
Jun	0.133	0.110	0.122	0.060	0.121	0.040	0.014	0.158	0.105	0.101	0.073	0.055	0.125	0.115
Jul	0.159	0.123	0.063	0.064	0.095	0.113	0.091	0.143	0.143	0.114	0.081	0.088	0.085	0.140
Aug	0.132	0.150	0.214	0.162	0.093	0.236	0.093	0.172	0.168	0.136	0.102	0.128	0.114	0.193
Sep	0.161	0.098	0.134	0.165	0.165	0.138	0.113	0.092	0.085	0.181	0.173	0.165	0.168	0.148
Oct	0.107	0.174	0.145	0.182	0.181	0.138	0.249	0.120	0.213	0.188	0.131	0.099	0.306	0.222
Nov	0.115	0.204	0.245	0.174	0.186	0.168	0.215	0.229	0.132	0.173	0.224	0.273	0.188	
Dec	0.239	0.124	0.285	0.211	0.180	0.287	0.120	0.080	0.213	0.278	0.205	0.181	0.172	

Table 2A: Radius of particulate-back of envelope calculation

Month	2000	2001	2002	2003	2004	2005	2006	2007	2008	2009	2010	2011	2012	2013
Jan		0.466	0.446	0.387	0.411	0.517	0.436	0.393	0.404	0.399	0.354	0.401	0.391	0.349
Feb		0.480	0.428	0.442	0.492	0.466	0.427	0.420	0.381	0.546	0.386	0.418	0.503	0.344
Mar	0.526	0.474	0.527	0.539	0.576	0.562	0.506	0.513	0.469	0.573	0.534	0.567	0.580	0.462
Apr	0.526	0.543	0.530	0.553	0.574	0.545	0.527	0.577	0.566	0.499	0.632	0.505	0.560	0.541
May	0.435	0.523	0.520	0.524	0.488	0.527	0.530	0.557	0.466	0.497	0.562	0.533	0.562	0.486
Jun	0.475	0.495	0.484	0.540	0.485	0.559	0.586	0.454	0.499	0.503	0.528	0.545	0.482	0.491

Jul	0.454	0.484	0.537	0.536	0.508	0.492	0.512	0.467	0.467	0.491	0.521	0.514	0.517	0.469
Aug	0.476	0.461	0.412	0.452	0.510	0.396	0.510	0.443	0.447	0.473	0.502	0.479	0.491	0.427
Sep	0.453	0.505	0.474	0.449	0.449	0.471	0.492	0.511	0.517	0.437	0.443	0.449	0.447	0.463
Oct	0.497	0.442	0.465	0.436	0.436	0.471	0.387	0.486	0.413	0.431	0.476	0.505	0.351	0.406
Nov	0.490	0.419	0.390	0.442	0.433	0.447	0.411	0.401	0.476	0.443	0.405	0.371	0.431	
Dec		0.482	0.364	0.414	0.437	0.362	0.486	0.521	0.413	0.368	0.418	0.437	0.443	

Table 3A: AOD statistics over Dori

Statistics	**2000**	**2001**	**2002**	**2003**	**2004**	**2005**	**2006**	**2007**	**2008**	**2009**	**2010**	**2011**	**2012**	**2013**
Number of values	10,000	12,000	12,000	12,000	12,000	12,000	12,000	12,000	12,000	12,000	12,000	12,000	12,000	10,000
Number of missing values	2,000	0,000	0,000	0,000	0,000	0,000	0,000	0,000	0,000	0,000	0,000	0,000	0,000	2,000
Minimum	0,222	0,275	0,165	0,206	0,256	0,163	0,207	0,219	0,196	0,173	0,150	0,178	0,145	0,136
Maximum	0,624	0,700	0,670	0,745	0,862	0,790	0,917	0,867	0,810	0,849	1,203	0,817	0,885	0,689
Mean	0,437	0,462	0,426	0,463	0,484	0,496	0,490	0,473	0,406	0,449	0,504	0,469	0,488	0,366
First quartile	0,363	0,395	0,278	0,325	0,320	0,374	0,306	0,307	0,260	0,312	0,258	0,295	0,321	0,246
Third quartile	0,509	0,519	0,613	0,674	0,553	0,668	0,596	0,586	0,475	0,523	0,645	0,614	0,682	0,468
Standard error	0,041	0,034	0,051	0,057	0,058	0,059	0,058	0,060	0,050	0,057	0,087	0,058	0,068	0,053
95% confidence interval	0,092	0,074	0,112	0,124	0,127	0,130	0,127	0,131	0,109	0,124	0,191	0,128	0,150	0,120
99% confidence interval	0,132	0,104	0,158	0,176	0,180	0,184	0,179	0,185	0,154	0,176	0,269	0,181	0,212	0,173
Variance	0,016	0,013	0,031	0,038	0,040	0,042	0,040	0,043	0,030	0,038	0,090	0,041	0,056	0,028
Average deviation	0,098	0,084	0,146	0,179	0,148	0,168	0,151	0,167	0,121	0,151	0,231	0,169	0,188	0,129
Standard deviation	0,128	0,116	0,176	0,196	0,200	0,205	0,200	0,207	0,172	0,196	0,300	0,201	0,236	0,168
Coefficient of variation	0,294	0,252	0,415	0,423	0,414	0,414	0,408	0,437	0,424	0,436	0,595	0,430	0,484	0,460
Skew	0,043	0,564	0,069	0,297	1,032	-0,023	0,501	0,608	1,136	0,660	1,066	0,181	0,350	0,326
Kurtosis	-0,447	0,558	-1,435	-1,862	0,277	-0,976	0,492	-0,452	1,633	0,216	1,363	-1,021	-0,908	0,216
Kolmogorov-Smirnov stat	0,124	0,169	0,167	0,284	0,191	0,148	0,141	0,129	0,186	0,174	0,136	0,134	0,142	0,159
Critical K-S stat, alpha=,10	0,369	0,338	0,338	0,338	0,338	0,338	0,338	0,338	0,338	0,338	0,338	0,338	0,338	0,369
Critical K-S stat, alpha=,05	0,409	0,375	0,375	0,375	0,375	0,375	0,375	0,375	0,375	0,375	0,375	0,375	0,375	0,409
Critical K-S stat, alpha=,01	0,489	0,449	0,449	0,449	0,449	0,449	0,449	0,449	0,449	0,449	0,449	0,449	0,449	0,489

It is observed that yearly corrosion rate has almost doubled since 2004. The highest corrosion rate is in 2006. Higher accuracy of the modified Faraday model can be achieved using ground dataset.

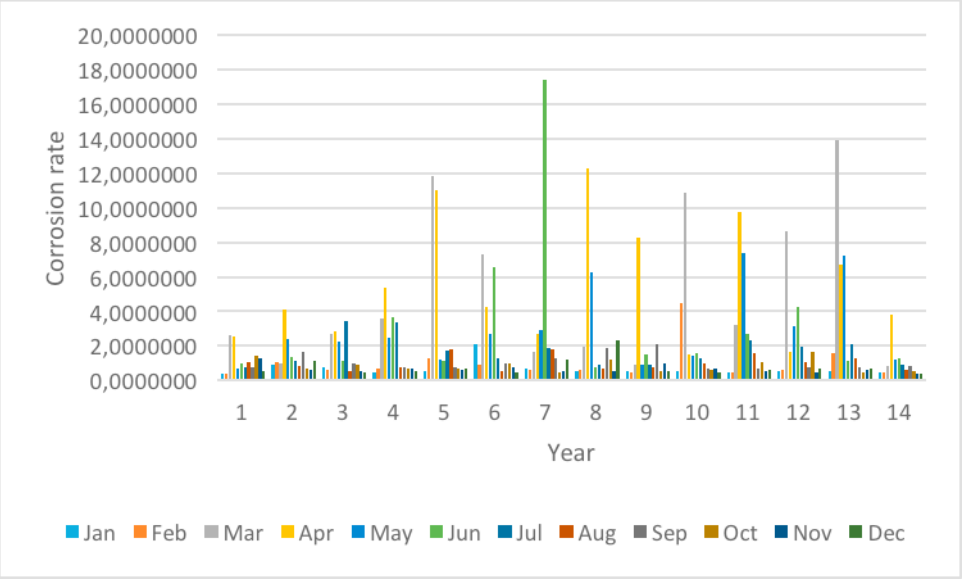

Figure 6: Yearly corrosion rate between 2000-2013

4. Conclusion

The yearly corrosion rate has almost doubled since 2004. Hence, atmospheric corrosion in regions of high aerosol loading is high. Higher accuracy of the modified Faraday model can be achieved using ground dataset.

Acknowledgements

The authors wish to appreciate their institutions. The authors acknowledge NASA for primary dataset.

References

[1]. Emetere Moses E., Akinyemi M.L. & Oladimeji T.E. (2016) Statistical Examination Of The Aerosols Loading Over Kano, Nigeria: The Satellite Observation Analysis, Scientific Review Engineering and Environmental Sciences, 72: 167-176
[2]. Emetere M.E., Akinyemi M.L., & Akinojo O., (2015) Parametric retrieval model for estimating aerosol size distribution via the AERONET, LAGOS station, Environmental Pollution, 207 (C), 381-390
[3]. Emetere, Moses Eterigho, (2016) Statistical Examination of the Aerosols Loading Over Mubi-Nigeria: The Satellite Observation Analysis, Geographica Panonica, 20(1), 42-50
[4]. Moses Eterigho Emetere, (2017). Investigations on aerosols transport over micro- and macro-scale settings of West Africa, Environ. Eng. Res., 22(1), 75-86
[5]. M. E. Emetere, (2017). Impacts of recirculation event on aerosol dispersion and rainfall patterns in parts of Nigeria, GLOBAL NEST JOURNAL 19 (2), 344-352
[6]. Rosa Vera, Diana Delgado, Blanca Rosales, Corros. Sci. 50 (2008) 1080-1098.
[7]. Rosa Vera, Patricia Verdugo, Marco Orellana, Eduardo Muñoz, Corros. Sci. 52 (2010) 3803-3810

[8]. H.C. Vasconcelos, B.M. Fernández-Pérez, J. Morales, R.M. Souto, S. González, V. Cano, and J.J. Santana (2014). Development of Mathematical Models to predict the Atmospheric Corrosion Rate of Carbon Steel in Fragmented Subtropical Environments, Int. J. Electrochem. Sci., 9: 6514 -6528

[9]. A.A. Kokhanovsky, W. Von Hoyningen-Huene, J.P. Burrows, Atmospheric aerosol load as derived from space, Atmospheric Research, 81 (2006), pp. 176-185

[10]. ASTM International, Volume 03.02, Standards G 5, G 48, G 59, G 61, G 102 (ASTM International, 2003: West Conshohocken, PA).